IEEE Access
Multidisciplinary | Rapid Review | Open Access Journal

Received February 4, 2020, accepted February 18, 2020, date of publication February 28, 2020, date of current version March 11, 2020.

Digital Object Identifier 10.1109/ACCESS.2020.2976713

Simulation Study on Static and Dynamic Characteristics of Electromagnet for Electro-Hydraulic Proportional Valve Used in Shock Absorber

FANGWEI XIE[1,2], RUI ZHOU[2], DENGSHUAI WANG[2], JUN KE[2], XINJIAN GUO[2], AND VAN XO NGUYEN[3]

[1]School of Mechatronic Engineering, China University of Mining and Technology, Xuzhou 221116, China
[2]School of Mechanical Engineering, Jiangsu University, Zhenjiang 212013, China
[3]Institute of Mechanical and Electrical Engineering, Hanoi University of Mining and Geology, Hanoi 90000, Vietnam

Corresponding author: Fangwei Xie (xiefangwei@163.com)

This work was supported by the Fundamental Research Funds for the Central Universities under Grant 2020ZDPYMS20.

ABSTRACT In order to improve the performance of the electromagnet for electro-hydraulic proportional valve used in shock absorber, the static and dynamic characteristics of the proportional electromagnet are simulated and analyzed, which provides theoretical basis for the design and optimization of structural parameters of the proportional electromagnet. In this paper, the magnetic circuit model and finite element simulation model of the proportional electromagnet used in shock absorber are established, and the Ansoft software is applied to analyze the influence of the key structural parameters of the proportional electromagnet on static output force and dynamic characteristics. The results demonstrate that with the increase of the depth of basin mouth, the effective travel of the proportional electromagnet increases, and the mean value of the electromagnetic force in the working range decreases. The larger the radial clearance between armature and guide sleeve is, the smaller the electromagnetic force in the effective travel is. When the depth of the basin mouth is 3.9 mm, the slope of the magnetic isolation ring is 35°, the chamfer length of the convex platform is 0.2 mm, and the radial clearance is 0.3 mm, the proportional electromagnet has good displacement-force and current-force characteristics. According to the further transient analysis, it is found that when the voltage amplitude is 24 V, the rise time of the electromagnetic force under step excitation signal is about 40 ms.

INDEX TERMS Proportional electromagnet, displacement-force characteristics, magnetic circuit model, shock absorber.

I. INTRODUCTION

The electro-hydraulic proportional valve used in the shock absorber can be applied to adjust the damping force, and improve the comfortability of the vehicle. As the key component of the electro-hydraulic proportional valve, the proportional electromagnet is widely used in electro-mechanical converter of electro-hydraulic proportional valve. Its function is to convert the input current signal into the output force and displacement signals. Its axial thrust is proportional to the coil current and keeps constant within the valid travel range. There are many structural parameters affecting the performance of the proportional electromagnets. The traditional design usually adopts empirical formulas, which makes the evaluation of the influences of each structural parameter is often not specific and accurate enough. Therefore, it is necessary to accurately analyze the effects of each parameter to provide a complete theoretical basis for performance optimization [1]. Institute of Hydrodynamic Driving, RWTH Aachen University, Germany [2], analyzed the influence of the helical tubular electromagnet including permeability, conductivity and eddy current effect on the output performance of electromagnet by the finite element analysis software. The analysis pointed out the relationship between the flux density and magnitude of electromagnetic force of helical tubular electromagnet. Liu *et al.* [3] analyzed the influences

The associate editor coordinating the review of this manuscript and approving it for publication was Jonghoon Kim.

of five factors, such as the length of the magnetic conductive material, the excitation current and the height of the iron core, etc. on the electromagnetic force of the proportional electromagnet with the simulation of the electromagnetic module in ANSYS software. The results demonstrate that for the direct-acting electromagnet, the magnitude of current shows the greatest effects on the electromagnetic force. Finally, they improved the performance of the electromagnet by optimizing the structure. Bayat *et al.* [4] established the electrodes and armature models of the proportional electromagnet for valves. Considering the non-linear effect, they used finite element analysis software to accomplish the simulation calculation, and finally obtained the static and transient indexes of the proportional electromagnet. Zhang and Xu [5] accomplished simulation analysis of a certain type of the proportional electromagnet by ANSYS software, and obtained the static magnetic force curves with the change of air gap under different parameters (angle of magnetic isolation ring, length and shape of armature, etc.). By comparison, they accomplished the improvement of the previous model. The performance of the optimized proportional electromagnet was significantly improved. According to the structural characteristics of the proportional electromagnet, Shao [6] put forward a kind of test bench based on LabVIEW, and designed the corresponding upper computer operation interface. Through test and analysis of a certain type of the proportional electromagnet, it is found that the test system is stable and reliable, and with a high test precision. Song *et al.* [7] established a model of the proportional electromagnet actuator (PEA) and analyzed the hysteresis principle, the results demonstrate that this control strategy can enhance the practicability and reliability of the long-stroke proportional electromagnet in case of position sensor fault and improve the position tracking performance during current closed-loop control. Lankin *et al.* [8] proposed a method about the analysis of the dynamic magnetization characteristics of the proportional electromagnets. The regression models were used to determine the electrical parameters of the components in the proportional electromagnet. The relation between the dynamic characteristics and the numerical values of the electrical parameters can be identified by this method. Liu *et al.* [9] independently designed a solenoid valve performance testing platform with a high level of automation. They adopted the input and output module to make up an open structure supervisory computer control system to realize the data preprocessing, sensor linearization and nonlinear compensation, scale transform and digital controller, which met the proportional solenoid valve testing requirements. Fu [10] proposed a new proportional electromagnetic dynamic vibration absorber (EDVA) to control of engine vibration during idling. The effectiveness of the hybrid proportional EDVA was evaluated through simulations and experiments under harmonic excitations in the 20-30 Hz frequency range. Both the simulation and measurements show that the hybrid proportional EDVA can yield the effective attenuation of the periodic idling vibration in the frequency range considered. Zhang *et al.* [11] proposed a novel pilot valve that employs two independent valve spools instead of the traditional port coupled valve spool. Due to the new structure, the influence of dead zone and damping on the performance of the valve is lightened; the dynamic characteristics and control accuracy of the valve are improved. Lu *et al.* [12] proposed an improved dead zone detection method to calibrate the pilot valve flow characteristics which include the micro flow rate. This new method avoids the threshold selection of the main valves pool displacement which affects the detected dead zone values. Its detection processes are realized. Yang *et al.* [13] used a hydraulic damper to enhance the increased force capacity of the small laboratory scale bio-inspired damper. The experimental results closely match the theoretical prediction of the damper with a consistent force output for these excitation frequencies. Agh *et al.* [14] introduced a new rotary proportional flow control valve. They replaced the more common hydro mechanical mechanisms with the direct drive actuation of flow control valve, and made the whole system lighter and cut down on the manufacturing cost.

In this paper, the finite element model of the proportional electromagnet is established, and Ansoft software is used to simulate and analyze the static force, firstly. The influence of the key structural parameters such as the depth of the basin mouth and the slope of the magnetic isolation ring on the electromagnetic force is studied to ensure that the proportional electromagnet has good current-force and displacement-force characteristics. Then, the transient characteristics of the proportional electromagnet are further simulated and analyzed, and the magnetic field and displacement-force under step voltage excitation are studied. The variation of the electromagnetic force, current and armature displacement with time is used to provide a theoretical basis for designing and optimizing the structural parameters of the proportional electromagnet.

II. STRUCTURE AND PRINCIPLE

With the action of the load spring, the proportional electromagnet can realize the damping adjustment of the shock absorber, which can be used to driving valve opening, spool position or travel control. The electromagnetic force of the ordinary proportional electromagnet varied with the gap, while that of the proportional electromagnet is nearly constant in the armature working range [15]. In short, the electromagnetic force of the proportional electromagnet is not related to the displacement of the spool, but only directly proportional to the excitation voltage or current. According to the principle of the minimum energy, it is found that the magnetic line of the proportional electromagnet always closes along the path of the minimum reluctance, and the magnetic line tends to shorten.

Figure 1 depicts that when a certain current is applied to the proportional electromagnet, the coil 4 generates magnetic potential and forms two magnetic loops ϕ_1 and ϕ_2 [16], [17]. The magnetic loop ϕ_1 penetrates the working air gap 9 from armature 8, enters the armature 8 axially, and then passes

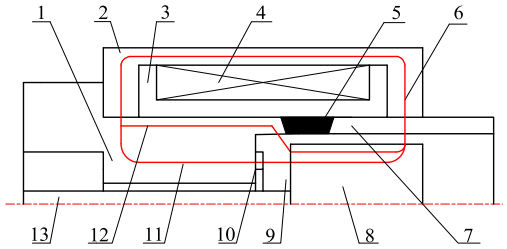

FIGURE 1. Proportional electromagnet magnetic circuit: 1. Pole-shoe; 2. Shell; 3. Coil skeletom; 4. Coil; 5. Magnetic isolation ring; 6. Magnetic line; 7. Guide sleeve; 8. Armature; 9. Air gap; 10. Limit piece; 11. ϕ_1; 12. ϕ_2; 13. Push rod.

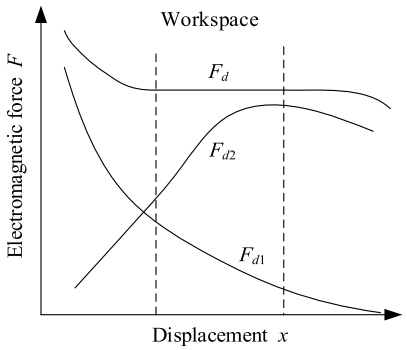

FIGURE 2. Displacement-force characteristic curve.

through the rear guide sleeve 7 and shell 2 to return to the pole-shoe 1 [18]. As the magnetic isolation ring 5 is not permeable, the magnetic loop ϕ_2 enters the armature 8 along the slope of the magnetic isolation ring 5, and then converges with the magnetic loop ϕ_1. Since the magnetic force line closes along the path with the minimum reluctance, and has a strong trend to shorten the closed path; simultaneously, the corresponding characteristics are obvious, and the magnetic loop ϕ_1 generates the axial electromagnetic attractive force F_{d_1}. The magnetic loop ϕ_2 produces a certain amount of additional axial force F_{d_2}. The resultant force of the two forces is the total output force F_d of the proportional electromagnet.

The displacement-force characteristic curve of the proportional electromagnet is demonstrated in Figure 2. The resultant force of F_{d_1} and F_{d_2} ensures F_d is an approximate horizontal line in the workspace.

III. MODELING PROCESS

A. MATHEMATICAL MODEL OF MAGNETIC FIELD

Maxwell equations are the basic equations describing general electromagnetic fields. Their differential forms can be expressed as:

$$\begin{cases} \text{rot}\, \boldsymbol{E} = -\dfrac{\partial \boldsymbol{B}}{\partial t} \\ \text{div}\, \boldsymbol{D} = \rho \\ \text{rot}\, \boldsymbol{H} = \boldsymbol{J} + \dfrac{\partial \boldsymbol{D}}{\partial t} \\ \text{div}\, \boldsymbol{B} = 0 \end{cases} \tag{1}$$

where, $\boldsymbol{B}$ is the magnetic flux density vector (T), $\boldsymbol{E}$ is the electric field intensity vector (V/m), $\boldsymbol{D}$ is the electric flux density (C/m^2), $\boldsymbol{H}$ is the magnetic field intensity vector (A/m), $\boldsymbol{J}$ is the conduction current density vector (A/m^2), ρ is the free charge density (C/m^3).

The relationships between field $\boldsymbol{E}$, $\boldsymbol{D}$, $\boldsymbol{H}$ and $\boldsymbol{B}$ are determined by the characteristics of magnetic medium. For linear medium, their relationships can be expressed as:

$$\begin{cases} \boldsymbol{D} = \varepsilon \boldsymbol{E} \\ \boldsymbol{B} = \mu \boldsymbol{H} \\ \boldsymbol{J} = \xi \boldsymbol{E} \end{cases} \tag{2}$$

where, ε is the dielectric constant of medium (F/m), μ is the permeability of medium (H/m), ξ is the dielectric conductivity (S/m).

For isotropic media, ε, μ and ξ are scalars; for anisotropic media, it is a tensor. The vector magnetic potential $\boldsymbol{A}$ is introduced [19], and the curl of $\boldsymbol{A}$ is used to express the magnetic flux density vector $\boldsymbol{B}$, then $\boldsymbol{B} = \text{rot}\, \boldsymbol{A}$. As is shown in Figure 3, when there is an external magnetic field, the resultant magnetic torque is not zero, and each vector in the magnetic field can be decomposed in three directions- circumferential p, radial q and axial z.

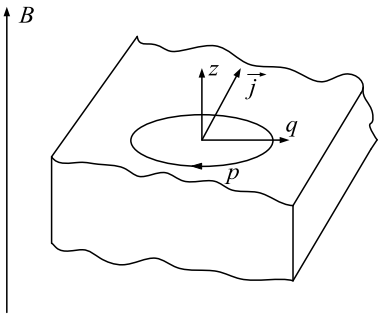

FIGURE 3. Decomposition model of each vector under the external magnetic field.

When the magnetic field of the proportional electromagnet is stable, the structure of the proportional electromagnet is axial symmetrical, thus when $\partial \boldsymbol{D}/\partial t = 0$, the vector magnetic potential $\boldsymbol{A}$ and the conduction current density vector $\boldsymbol{J}$ are parallel, then,

$$\begin{cases} \boldsymbol{A}_p = \boldsymbol{A}, \quad \boldsymbol{A}_z = \boldsymbol{A}_q = 0 \\ \boldsymbol{J}_p = \boldsymbol{J}, \quad \boldsymbol{J}_z = \boldsymbol{J}_q = 0 \end{cases} \tag{3}$$

Since $\boldsymbol{B} = \mu \boldsymbol{H}$, which can be substituted into Eq. (1), and the results can be expressed as:

$$\text{rot}(\text{rot}\boldsymbol{A}/\mu) = \boldsymbol{J} \tag{4}$$

Since the components of $\boldsymbol{J}$ in radial q and axial z are zero, the Eq. (4) is written in the form of components in three directions- circumferential p, radial q and axial z, as follows,

$$\frac{\partial}{\partial q}\left[\frac{1}{q\mu_z}\frac{\partial (q\boldsymbol{A})}{\partial q}\right] + \frac{\partial}{\partial z}\left(\frac{1}{\mu_q}\frac{\partial \boldsymbol{A}}{\partial z}\right) = -\boldsymbol{J} \tag{5}$$

For the proportional electromagnet, there are two boundary conditions for the above equations [20]. One exists on the surface of the air dielectric layer around the proportional electromagnet $\mathbf{\Gamma_1}$, and the other exists on the normal derivative $\mathbf{\Gamma_2}$ of the z axis (vector magnetic potential $\boldsymbol{A}$). The formulas of the above two boundary conditions can be obtained:

$$\mathbf{\Gamma_1}: \boldsymbol{A}(q, z) = 0 \tag{6}$$

$$\mathbf{\Gamma_2}: \partial \boldsymbol{A}(q, z)/\partial z = 0 \tag{7}$$

The static attraction of the proportional electromagnet depends on the magnitude of the steady magnetic field. Eqs. (3), (4) and (5) all describe the steady-state characteristics of the magnetic field of the proportional electromagnet. Therefore, the above three equations are also the basic equations that followed by the Ansoft Maxwell.

B. STRUCTURE MODEL OF RELUCTANCE

The magnitude of magnetic flux depends on the Ampere turns and magnetic circuit reluctance. When the Ampere turns of the proportional electromagnet are constant, the magnetic flux in the magnetic circuit is most affected by the reluctance. Therefore, it is necessary to calculate the reluctance of each part of the magnetic circuit. In order to study the reluctance distribution conveniently, the internal magnetic circuit structure of the designed proportional electromagnet is divided, which is shown in Figure 4.

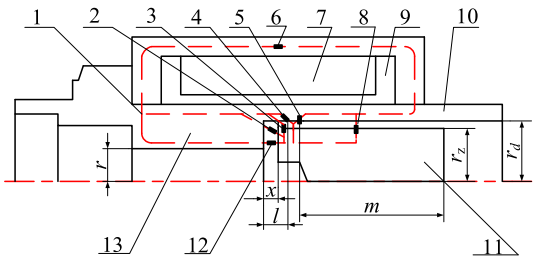

FIGURE 4. Reluctance analysis of the proportional electromagnet: 1. Shell; 2. R_3; 3. R_4; 4. R_5; 5. R_6; 6. R_1; 7. Coil; 8. R_7; 9. Coil skeleton; 10. Sleeve; 11. Armature; 12. R_2; 13. Pole-shoe.

In order to depict the regular reluctance conveniently, the relevant structure of the proportional electromagnet is specified as follows, which is clearly shown in Figure 5.

1) R_1

R_1 is a non-air-gap reluctance, specifically referring to the sum of the reluctance of high permeability materials such as shell, pole-shoe and guide sleeve. Apart from air gap, the shell, pole-shoe and other components of proportional electromagnet is connected closely, the magnetic circuit has not been interrupted, and there is no magnetic leakage phenomenon in the material interior and the joint, so the value of R_1 can be neglected, and the reluctance mainly exists in the air gap.

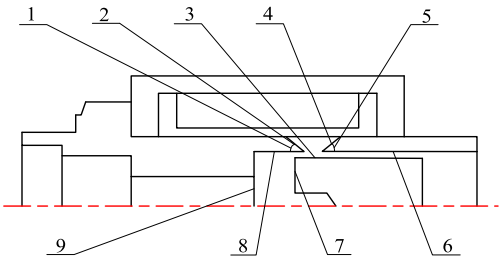

FIGURE 5. Schematic diagram of the reluctance structure of the proportional electromagnet: 1. Front end face of magnetic isolation angle; 2. Front end face of magnetic isolation ring; 3. Armature side; 4. Rear end face of magnetic isolation ring; 5. Rear end face of magnetic isolation angle; 6. Inner side of rear guide sleeve; 7. End face of armature; 8. Inner side of front guide sleeve; 9. End face of pole-shoe.

2) R_2, R_4, R_7

R_2, R_4 and R_7 are regular reluctances, and their expressions are as follows:

$$R = \frac{d}{\mu S} \tag{8}$$

where, d is the length of magnetic medium (m), μ is the permeability of magnetic medium (H/m), S is the equivalent cross-sectional area of magnetic medium (m^2).

R_2 is the main air gap reluctance, its shape is the hollow cylinder formed by the combination of the pole-shoe end face, guide rod, guide sleeve and armature end face. Its interior is filled with oil, which can be expressed as:

$$R_2 = \frac{x}{\mu_0 \mu_k \pi (r_z^2 - r^2)} \tag{9}$$

where, μ_0 is the permeability of magnetic medium in the air (H/m), μ_k is the relative permeability of magnetic medium (no-dimension). The shape of R_4 is similar to that of R_1. The magnetic force line enters the armature from the inner surface of the rear guide sleeve through the radial clearance. Its expression can be described as:

$$R_4 = \frac{r_d - r_z}{2\mu_0 \mu_k \pi r_z (l - x)} \tag{10}$$

Similar to R_4, R_7 is a reluctance consisting of the clearance between the side of armature and the inside of rear guide sleeve, and its shape is similar to that of a hollow cylinder. The magnetic force line reaches the inner wall of rear guide sleeve along the radial direction of armature.

$$R_7 = \frac{r_d - r_z}{2\mu_0 \mu_k \pi r_z m} \tag{11}$$

When the armature is attracted by the electromagnetic force to overcome spring resistance and move toward the pole-shoe, the axial clearance between armature and pole-shoe decreases. According to the above formulas, it can be found that R_2 decreased linearly; $l - x$ increases gradually, the area corresponding to the front sleeve side and the side of armature increases, R_4 decreases gradually; m decreases gradually, and the area corresponding to the side of rear guide sleeve and side of armature decreases. According to the formula, R_7 also increases gradually.

3) R_3, R_5, R_6

R_3, R_5 and R_6 are irregular reluctances. R_3 is the reluctance produced by the armature end face and the inner side of the front guide sleeve. These two ends are perpendicular to each other. The shape of the magnetic force line is very complex. The magnitude of the reluctance is non-linear with the displacement, and there is no specific expression. But according to the property of the reluctance, it can be inferred that when the armature is far away from the pole-shoe, the value of R_3 remains approximately unchanged; when the armature moves toward right to x_1, the axial gap between the armature end face and the pole-shoe decreases, R_3 will decrease rapidly. The trend diagram of R_3 is shown in Figure 6.

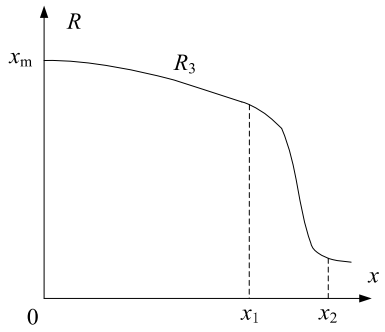

FIGURE 6. Schematic diagram of the reluctance change trend.

R_5 and R_6 are related to the shape of the front and rear end faces of the magnetic isolation ring. The magnetic circuit structure is more complicated, and it is difficult to express via accurate mathematical formulas. Generally, the motion range of armature x is less than l, therefore, it can be considered that when the armature is at any position within the motion range, the structural form of R_5 and R_6 is basically unchanged; meanwhile, the magnitude of R_5 and R_6 remains approximately unchanged.

Although it is difficult to express the above-mentioned irregular reluctance by accurate mathematical formulas, the air gap that forms the reluctance is larger, hence, we can consider approximately that R_3 and R_5 are much larger than R_4, and R_6 is much larger than radial reluctance R_7. The equivalent magnetic circuit inside the proportional electromagnet can be described by the above analysis of the reluctance, which can be described in Figure 7.

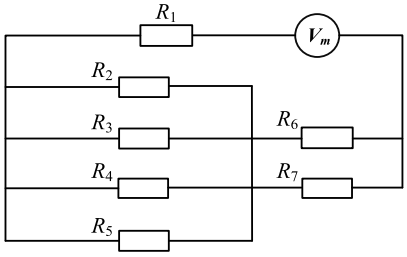

FIGURE 7. Proportional electromagnets equivalent magnetic circuit.

R_2, R_3, R_4 and R_5 are parallel reluctance, and their sum of parallel reluctance can be expressed as R_{25}:

$$\frac{1}{R_{25}} = \frac{1}{R_2} + \frac{1}{R_3} + \frac{1}{R_4} + \frac{1}{R_5} \tag{12}$$

R_6 and R_7 are parallel reluctance, and their sum of parallel reluctance can be expressed as R_{67}:

$$\frac{1}{R_{67}} = \frac{1}{R_6} + \frac{1}{R_7} \tag{13}$$

Since R_7 is very small, and R_6 is much larger than R_7, the influence of R_6 on R_{67} can be neglected. Similarly, R_{67} is much smaller than R_{25}, and there are few changes in armature movement. Therefore, the influence of R_2, R_3, R_4 and R_5 on the flux variation is mainly considered when studying the electromagnetic force of the proportional electromagnet, and the main factors affecting the magnitude of these reluctance are the size of air gap, depth of basin mouth, slope of magnetic isolation ring, chamfer angle, radial clearance between armature and guide sleeve, etc. [21].

C. ANSOFT SIMULATION MODEL AND PARAMETER SETTING

Ansoft Maxwell software is a widely used in the electromagnetic analysis. The simulation process is shown in Figure 8.

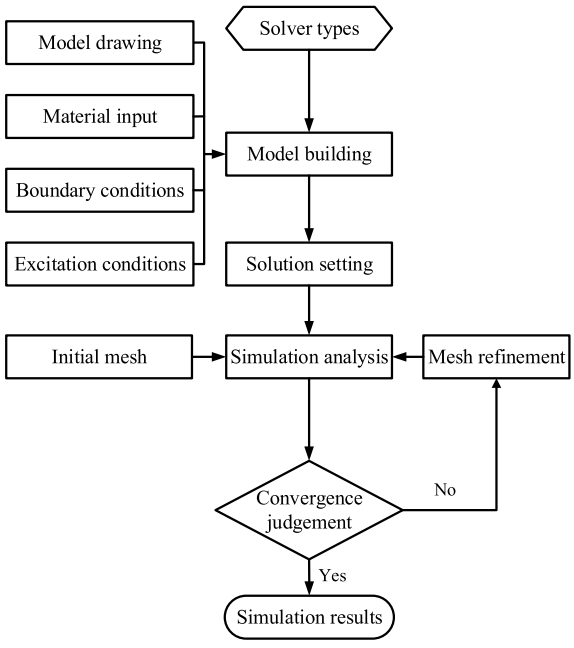

FIGURE 8. Simulation process.

The specific simulation steps are as follows:

1) SOLVER TYPES

The proportional electromagnet in this simulation is a direct-acting electromagnet with a rated voltage of 24V DC. The static magnetic field solver is used to analyze the proportional electromagnet.

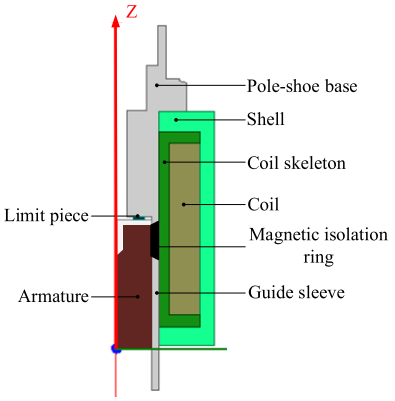

FIGURE 9. Proportional electromagnet simulation model.

TABLE 1. Material of various components of proportional electromagnet.

Part names	Materials
Shell, Pole-shoe, Armature, Guide sleeve	Pure iron(DT4)
Magnetic isolation ring	Tin bronze
Coil	Enameled copper wire
Coil skeletons	Poly tetra fluoroethylene
Filler	Oil

2) MODEL BUILDING AND PARAMETER SETTING

The designed proportional electromagnet has a centrosymmetric structure. In order to save computing resources and shorten computing time, a 2D plane model of the proportional electromagnet is established, which is shown in Figure 9, the simulation is carried out by using Ansoft Maxwell 2D module.

The material of each component of the proportional electromagnet is shown in Table 1, where the tin bronze, poly tetra fluoroethylene, oil and other materials are self-contained in the software material library, and their *B-H* curves can be directly used. Electrical pure iron [22] (DT4) has a good magnetic conductivity, and its saturated magnetic induction strength is greater than 2.15 T. Electrical pure iron is not included in the material library. It is necessary to define the magnetic conductivity, conductivity and density of electrical pure iron manually. The magnetization curve of DT4 is non-linear [23], with a good magnetic conductivity of 7690000 S/m and density of 7870 kg/m^3.

3) SETTING OF EXCITATION SOURCES

The excitation source is selected as the current source, and the value of the current source is the magnetic potential of the coil, which is equal to the product of the coil current and the number of the coil turns. According to the magnetic potential equation, the ampere-turn number of coil *IN* can be deduced:

$$IN = 0.106 B_P \mu_a \delta_1 \tag{14}$$

where, δ_1 is the sum of the thickness of the magnetic isolation sheet and the effective working travel of the armature (mm), μ_a is the air gap magnetic conductivity coefficient (H/m), B_p is the air gap magnetic induction intensity (Gs). The initial value of δ_1, μ_a, B_p in this simulation are set as 0.3 mm, 0.3 H/m, 12000 Gs, respectively.

When the above initial values are substituted into Eq. (14), the value of *IN* can be obtained as 1144.8 AN, and take the integral value of *IN* as 1145 AN.

4) BOUNDARY CONDITIONS

The solver of static magnetic fields in the Ansoft Maxwell software contains many kinds of boundary conditions, among which the balloon boundary condition is one of the most commonly used. With the setting of balloon boundary condition, the problem that the drawing solution area of the designed model is excessively large can be effectively avoided. The simulation time and consumption of computing resources can be further reduced, thus simulation efficiency can be greatly improved. Therefore, the balloon boundary condition is adopted in this model.

5) MESHING

The interior of this model is meshed, the maximum side length of the mesh triangle element of the guide sleeve, magnetic isolation ring and armature is 0.5 mm, the maximum side length of other parts is 0.8 mm. The software will automatically mesh the model, which is shown in Figure 10. If the mesh of the model is not sufficiently fine and dense, which will result in the non-convergence of the calculation results, and the system will automatically thicken the mesh of the key areas.

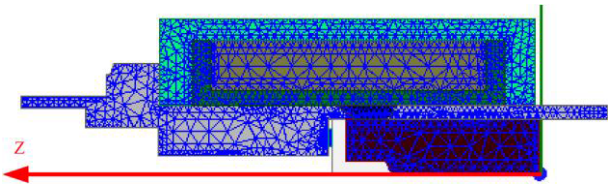

FIGURE 10. Simulation model meshing.

6) SOLVER SETTINGS

The solver of static magnetic field is selected in this model. When the error variation obtained by the iterative calculation is less than the set value or the number of iterative steps reaches the set value, the calculation ends. The calculation results can be expressed in the form of curves and displayed in an intuitive way. The specific settings of the solver are shown in Table 2.

IV. STATIC CHARACTERISTIC ANALYSIS

The shape of the basin mouth, the slope of the front magnetic isolation ring, the chamfer length of the magnetic isolation ring, the radial clearance between armature and the guide sleeve has great influences on the electromagnetic suction

TABLE 2. Solver settings.

Solution option	Parameter settings
Solver types	Static magnetic field
Maximum convergence steps	10 steps
Convergence error	1%
Refinement per pass	30%
Nonlinear residual error	0.0001

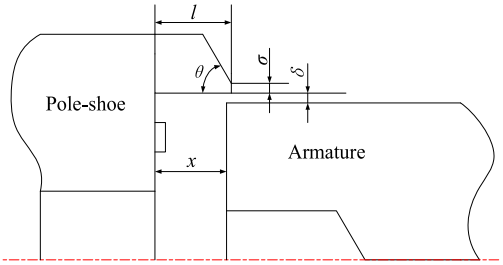

FIGURE 11. Structural parameters of the proportional electromagnet.

characteristics [24]. The values of l, θ, σ and δ respectively represent the depth of the basin mouth, the slope of the magnetic isolation ring, the chamfer length and the radial clearance between armature and guide sleeve, which are shown in Figure 11.

A. INFLUENCE OF THE DEPTH OF BASIN MOUTH ON ELECTROMAGNETIC FORCE

The initial parameters of the model are that $\theta = 35°$, $\sigma = 0$ mm, $\delta = 0.3$ mm. The effects of different depth of the basin mouth l on the electromagnetic force are studied. The simulation results are shown in Figure 12.

As is shown in Figure 12(a), with the increase of the depth of the basin mouth l, the tail inflection point of the displacement-force characteristic curve of the proportional electromagnet gradually moves toward the right, and the effective working space of the armature increases ($x \leq 2$mm), but with the increase of l, the value of the electromagnetic force in the working space decreases gradually. Figure 12(b) shows that the electromagnetic force of the armature in the effective travel interval decreases with the displacement, and the smaller the depth of the basin mouth is, the steeper the displacement-force characteristic curve is [25]. When the depth of the basin mouth is equal to 4.1 mm, the displacement-force characteristic of the armature is the best in the effective travel interval, but the electromagnetic force is the smallest in the travel interval, whose mean value is about 78 N.

B. INFLUENCE OF THE SLOPE OF THE MAGNETIC ISOLATION RING ON ELECTROMAGNETIC FORCE

Taking the structural parameters of the basin opening depth $l = 3.9$ mm, the chamfer length of the convex platform

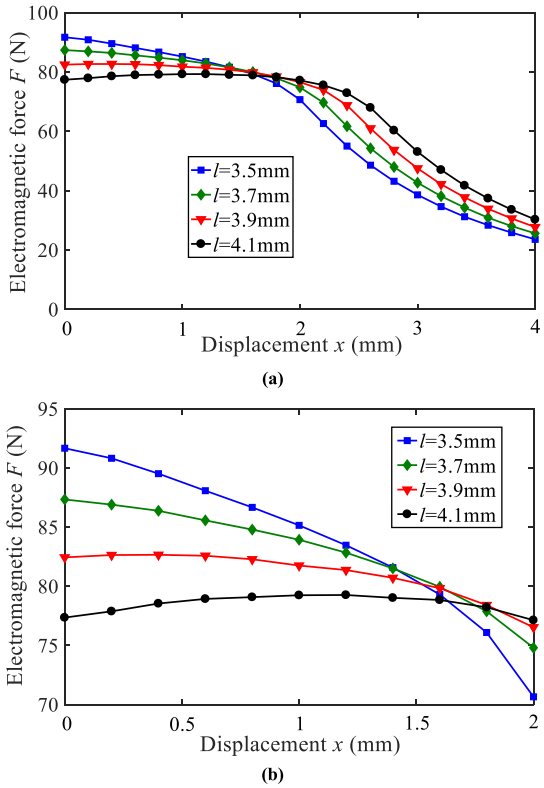

FIGURE 12. Influence of the basin mouth depth on electromagnetic force characteristics: (a) Displacement interval 0-4mm; (b) Displacement interval 0-2mm.

$\sigma = 0$ mm and radial clearance between armature and guide sleeve $\delta = 0.3$ mm as the research object, the influence of the slope of the magnetic isolation ring on electromagnetic field θ is further studied. The simulation results are shown in Figure 13.

It can be seen from the Figure 13(b) that within the working range of armature ($0 \sim 2$mm), the slope θ mainly affects the slope of the electromagnetic force, and the electromagnetic force curves under different influences almost intersect at the same point. When $\theta = 33°$, the electromagnetic force decreases gradually in the working range, and the difference value between the maximum value and the minimum value reaches 8 N. When θ increases gradually, the displacement-force characteristics of electromagnetic force gets improved. When the slope θ is greater than 35°, the electromagnetic force increases first, and then decrease with the changes of displacement; when $\theta = 35°$, the electromagnetic force has better displacement-force characteristics in the first half of the working interval, and the value of the electromagnetic force in the second half decreases slightly.

C. INFLUENCE OF THE CHAMFER LENGTH OF THE CONVEX PLATFORM ON ELECTROMAGNETIC FORCE

The influence of the chamfer length of the convex platform σ on electromagnetic force is further studied by taking the structural parameters of the depth of the basin mouth

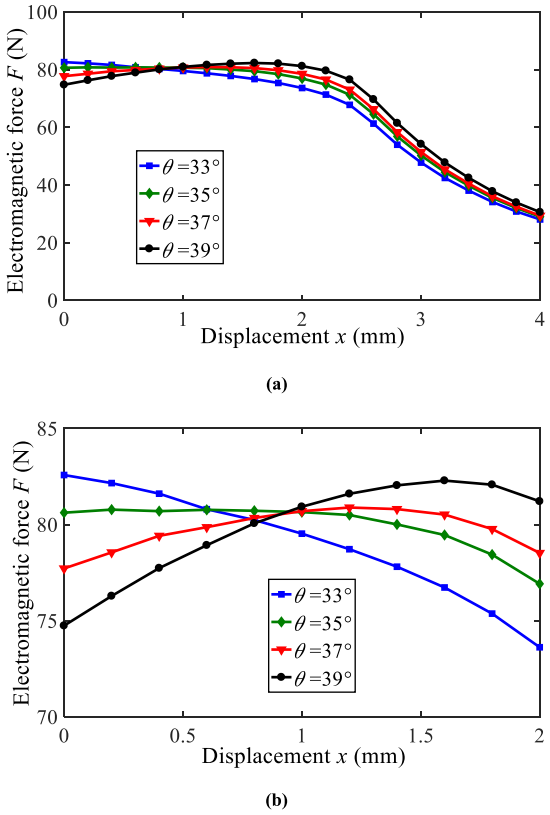

FIGURE 13. Influence of the slope of the magnetic isolation ring on the displacement-force characteristics: (a) Displacement interval 0-4mm; (b) Displacement interval 0-2mm.

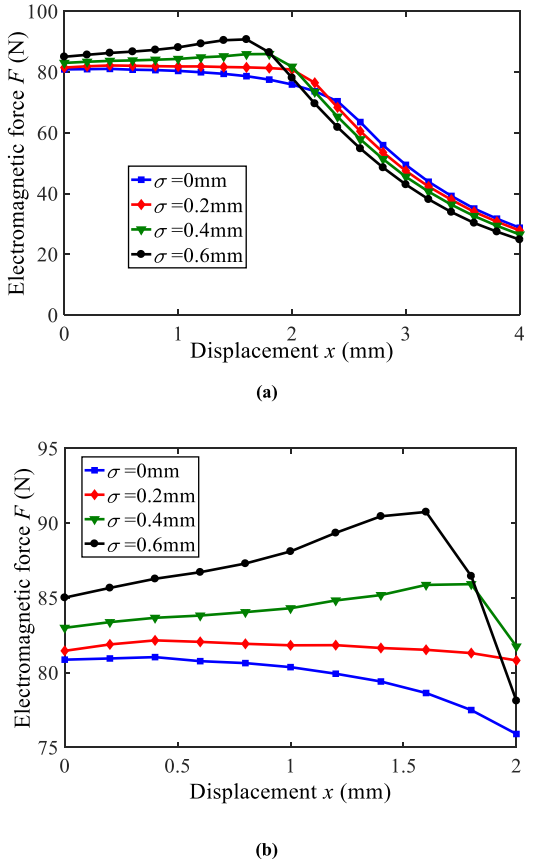

FIGURE 14. Influence of the chamfer length of the convex platform on displacement-force characteristics: (a) Displacement interval 0-4mm; (b) Displacement interval 0-2mm.

$l = 3.9$ mm and the slope of the magnetic isolation ring $\theta = 35°$ as research object. The simulation results are shown in Figure 14.

Figure 14(a) shows that with the increase of the chamfer length of the convex platform σ, the electromagnetic attraction of the armature at the displacement of 2 mm gradually increases, and then with the increase of the displacement, the electromagnetic force drops sharply. From Figure14(b), it can be found that when $\sigma = 0.2$ mm, the levelness of electromagnetic attraction of the armature is the best in the working range, and the difference value between the maximum and minimum electromagnetic force is only 1 N in the working range of the armature.

D. INFLUENCE OF THE RADIAL CLEARANCE BETWEEN ARMATURE AND GUIDE SLEEVE ON ELECTROMAGNETIC FORCE

After the above simulation analysis, the structural parameters of the basin mouth are obtained: the depth of the basin mouth l is 3.9 mm, the front slope of the magnetic isolation ring θ is 35°, and the chamfer length of the convex platform σ is 0.2 mm. The influence of the radial clearance between the armature and the guide sleeve on the electromagnetic attraction δ will be further investigated [26]. Taking $\delta = 0.3$ mm, 0.32 mm, 0.34 mm and 0.36 mm as test value respectively, the simulation results are shown in Figure 15.

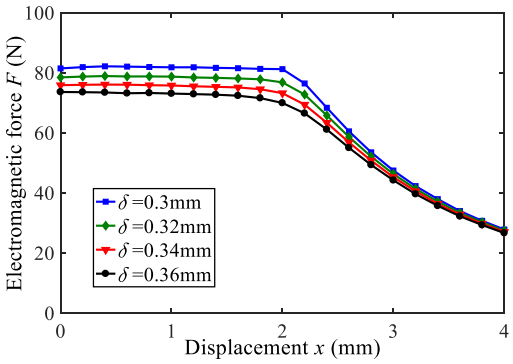

FIGURE 15. Influence of the radial clearance on displacement-force characteristics.

It can be revealed from the Figure 15 that the radial clearance between armature and guide sleeve δ mainly affects the mean value of electromagnetic attraction on armature, and the change of δ will not affect the displacement-force characteristics of electromagnetic force. The bigger the armature δ is, the smaller the electromagnetic force is. When $\delta = 0.3$ mm, F reaches 82 N, when $\delta = 0.36$ mm, F is

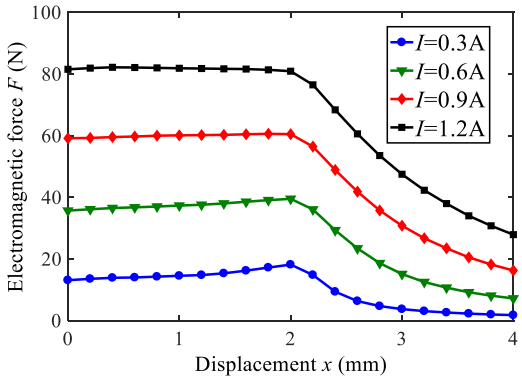

FIGURE 16. Displacement-force characteristics.

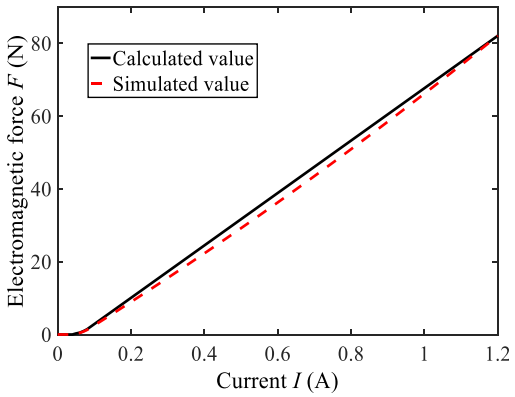

FIGURE 17. Current-force characteristics.

only about 74 N. When δ increases by 0.02 mm on average, the electromagnetic force of the armature decreases by about 2 N in the working space. Therefore, in order to meet the requirements of the design, the radial clearance between the armature and the guide sleeve δ should not be greater than 0.3 mm.

E. VERIFY THE IMPROVED MODEL

Considering the displacement-force characteristics and the force mean value in the working space, the key structural parameters of the proportional electromagnet [27], [28] are finally determined. The depth of the basin mouth l is 3.9 mm, the slope of the magnetic isolation ring θ is 35°, the chamfer length of the convex platform σ is 0.2 mm, and the radial clearance between armature and guide sleeve δ is 0.3 mm.

When the coil current I is set as 0.3A, 0.6A, 0.9A and 1.2A respectively, the electromagnetic force is parameterized and simulated, and the simulation results of the displacement-force characteristics are shown in Figure 16. The displacement-force characteristic curves are approximately horizontal under different driving currents, and the distribution is symmetrical.

The current-force characteristics of the proportional electromagnet are studied by selecting the position of the armature with 1 mm displacement and setting the current of the exciting power source to change from 0 to 1.2 A [29]. Figure 17 depicts that the calculated and simulated curves of the current-force characteristics almost coincide with each other, which shows that the proportional electromagnet model has good current-force characteristics and the values of relevant parameters are rational.

V. DYNAMIC CHARACTERISTIC ANALYSIS

When the proportional electromagnet is electrified, the armature moves in a straight line in the guide sleeve. The magnetic field, force, energy and speed are all defined as functions of time [4]. The ampere turns of the proportional electromagnet are variables in the whole process. The transient simulation analysis of the proportional electromagnet is conducted in Ansoft Maxwell software.

The motion of armature under the excitation of step signal is a kind of suction motion, which includes the time period of suction-touch stage and suction-move stage [30]. The suction-touch stage is generally expressed by the touch time, which refers to the time taken by the coil from the beginning of the excitation voltage to the time when the current increases exponentially to the attract current (attract current: The current when the electromagnetic force is equal to the initial resistance of the armature). The change of the current and magnetic field is more complicated after entering the movement stage. With the movement of the armature, the air gap reluctance changes significantly. Back electromotive force produced by the self-inductance of the coil counteracts the original electromotive force and inhibits the further increase of current; when the coil current increases to a certain extent and then stops growing or even slightly decreasing. When the armature moves to the specified position [31], and stops moving, and then the air-gap reluctance does not change, the coil current rises to a steady-state current again in accordance with the new exponential growth mode. Hence, the movement time of armature is often less than the stability time of magnetic field and electromagnetic force.

The electromagnetic force-time characteristic curves under different voltage excitation conditions are shown in Figure 18. When the excitation voltage is 24 V, the steady-state value of electromagnetic force is 82 N and the stable time is about 40 ms. When the excitation voltage is 8 V, the steady-state value of the electromagnetic force is about 20 N, and the steady-state time is close to 100 ms. The above analysis demonstrates that the larger the excitation voltage is, the larger the steady-state electromagnetic force is, the shorter the triggering time and moving time of armature is. From a single curve, when the excitation voltage is obtained, the electromagnetic force increases first, then decreases, and then continues to increase to a stable value. The larger the voltage is, the more obvious the trend of current increases first and then decreases. That is because with the increase of magnetic field intensity, the electromagnetic force overcomes the load force, and the armature begins to move at that time, which results in the production of the back electromotive force in

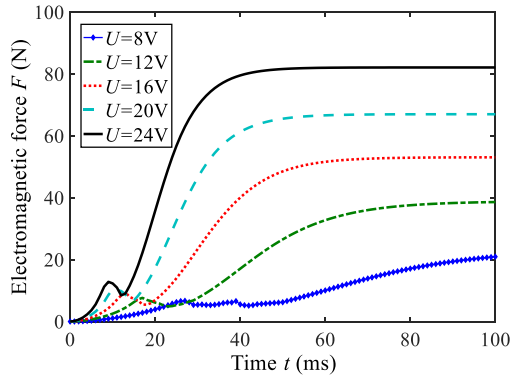

FIGURE 18. Force-time transient characteristics.

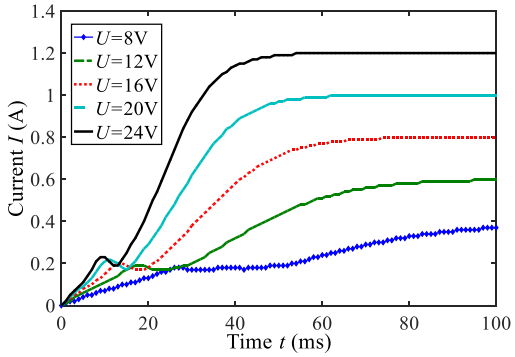

FIGURE 19. Current-time transient characteristics.

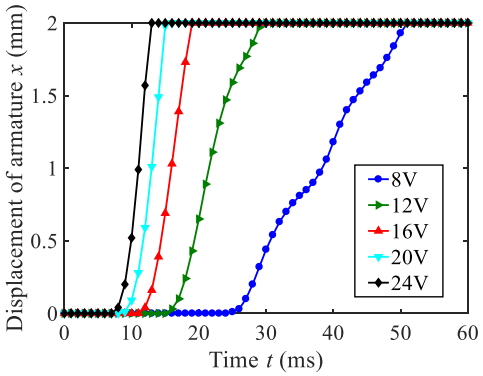

FIGURE 20. Displacement-time transient characteristics of the armature.

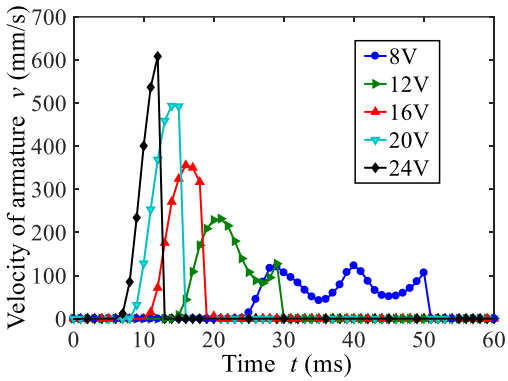

FIGURE 21. Velocity-time transient characteristics of the armature.

the coil, thus restraining the growth of the magnetic force. When the armature stops moving, the magnetic potential will be established continually in the magnetic circuit, and the electromagnetic force will increase gradually until the magnetic field is stable, and then the electromagnetic force will be not change.

The current-time characteristic curve under different voltage excitation conditions [32] is shown in the Figure 19. The change trend of the current with time is consistent with that of electromagnetic force. The larger the voltage is, the shorter the time for current to reach stable state is, and the larger the current flows through the coil. When the excitation voltage is 24 V, the current stability time is about 40 ms and the steady-state current is 1.2 A.

The influence of the excitation voltage on the displacement-time characteristics of the proportional electromagnet is shown in Figure 20. It can be revealed from the figure that when the armature weight, load force, motion damping and coil resistance are determined, the larger the coil voltage is, the shorter the time of armature movement is. The shortest time of armature movement under the excitation voltage of 24 V is about 5 ms, and the longest time of armature movement under the excitation voltage of 8 V is about 20 ms.

The influence of the excitation voltage on the velocity-time characteristics of armature is shown in Figure 21. It can be revealed from the figure that with a higher voltage, the armature moves to its peak speed faster. When the excitation voltage is 8 V and 12 V, the armature movement velocity is smaller and fluctuated. This is because the electromagnetic force under the low voltage condition is smaller, which is not enough to completely suppress the load resistance.

VI. CONCLUSION

In this paper, the influence of the structural parameters of the proportional electromagnet on the displacement-force characteristics of the proportional electromagnet is studied. The improved parameter model is verified and the dynamic characteristics simulation of the model is also carried out. The main conclusions are summarized as follows:

(1) With the increase of the depth of the basin mouth, the effective travel of the proportional electromagnet increases, and the mean value of the electromagnetic force in the working space decreases; the larger the radial clearance between armature and guide sleeve is, the smaller the electromagnetic force in the effective travel is.

(2) When the depth of the basin mouth is 3.9 mm, the slope of the magnetic isolation ring is 35°, the chamfer length of the convex platform is 0.2 mm, and the radial clearance is 0.3 mm, the proportional electromagnet has good displacement-force and current-force characteristics, which can meet the general application requirements of the shock absorber.

(3) When the armature weight, load force, motion damping and coil resistance are determined, the larger the coil voltage is, the shorter the time of armature movement is. The shortest time of armature movement under the excitation voltage of 24 V is about 5 ms.

REFERENCES

[1] Y. F. Yuan, G. L. Tao, H. Liu, and W. Ban, "Study of a bidirectional proportional electromagnet," *Appl. Mech. Mater.*, vols. 278–280, pp. 155–158, Jan. 2013.
[2] A. Schultz, "Design of valve solenoids using the method of finite elements," *J. Power Transmiss. Motion Control*, vol. 187, no. 12, pp. 243–254, 2005.
[3] Q. F. Liu, H. L. Bo, and B. K. Qin, "Sensitivity analysis of design parameters of direct solenoid valves," (in Chinese), *J. Nucl. Power Eng.*, vol. 30, no. 5, pp. 96–100, 2009.
[4] F. Bayat, A. F. Tehrani, and M. Danesh, "Finite element analysis of proportional solenoid characteristics in hydraulic valves," *Int. J. Automot. Technol.*, vol. 13, no. 5, pp. 809–816, Jul. 2012.
[5] L. W. Zhang and Y. M. Xu, "Finite element magnetic analysis of proportional electromagnets," (in Chinese), *J. Mach. Tools Hydraulic Pressures*, vol. 41, no. 17, pp. 169–170, 2013.
[6] F. Shao, "Development of the magnetic characteristic test system for proportional electromagnet," (in Chinese), *J. Manuf. Autom.*, vol. 40, no. 4, pp. 99–101, 2018.
[7] E.-Z. Song, G.-F. Zhao, C. Yao, Z.-K. Ma, S.-L. Ding, and X.-Z. Ma, "Study of nonlinear characteristics and model based control for proportional electromagnet," *Math. Problems Eng.*, vol. 2018, pp. 1–11, Sep. 2018, doi: 10.1155/2018/2549456.
[8] A. M. Lankin, N. I. Gorbatenko, and M. V. Lankin, "Dynamic magnetization characteristics of proportional electromagnets," *Russian Eng. Res.*, vol. 38, no. 9, pp. 731–732, Oct. 2018.
[9] J. Liu, W. Jiang, and Y. Li, "The design of electric control system of proportional electromagnetic valve test bench," *Adv. Eng. Res.*, vol. 86, pp. 120–122, Jan. 2017.
[10] T. Fu, "A novel kind of proportional electromagnetic dynamic vibration absorber," SAE Tech. Papers 2019-01-1586, Jun. 2019, doi: 10.4271/2019-01-1586.
[11] J. Zhang, Z. Lu, B. Xu, and Q. Su, "Investigation on the dynamic characteristics and control accuracy of a novel proportional directional valve with independently controlled pilot stage," *ISA Trans.*, vol. 93, pp. 218–230, Oct. 2019, doi: 10.1016/j.isatra.2019.03.023.
[12] Z. Lu, J. Zhang, B. Xu, D. Wang, Q. Su, J. Qian, G. Yang, and M. Pan, "Deadzone compensation control based on detection of micro flow rate in pilot stage of proportional directional valve," *ISA Trans.*, vol. 94, pp. 234–245, Nov. 2019, doi: 10.1016/j.isatra.2019.03.030.
[13] H. T. Yang, I. Y. Kwon, C. J. Randall, P. K. Hansma, and F. S. Ly, "Preliminary design, experiment, and numerical study of a prototype hydraulic bio-inspired damper," *J. Sound Vib.*, vol. 459, Oct. 2019, Art. no. 114845.
[14] S. M. Agh, J. Pirkandi, M. Mahmoodi, and M. Jahromi, "Optimum design, simulation and test of a new flow control valve with an electronic actuator for turbine engine fuel control system," *Flow Meas. Instrum.*, vol. 65, pp. 65–77, Mar. 2019.
[15] Y. Kawase and Y. Ohdachi, "Dynamic analysis of automotive solenoid valve using finite element method," *IEEE Trans. Magn.*, vol. 27, no. 5, pp. 3939–3942, Sep. 1991.
[16] O. Maloberti, O. Mansouri, D. Jouaffre, M. Hamzaoui, J. Derosiere, N. Buiron, P. Sansen, T. Sapanathan, P. Pelca, M. Rachik, J.-P. Leonard, G. Lembrouck, D. Haye, and A. Macret, "Analytical design model of coil parameters for the electro-magnetic forming technology–case of the 1-turn coil dedicated to tubular parts forming and crimping with 1D approximation," *J. Mater. Process. Technol.*, vol. 266, pp. 450–473, Apr. 2019.
[17] L. Qiu, C. Wang, A. Abu-Siada, Q. Xiong, W. Zhang, B. Wang, N. Yi, Y. Li, and Q. Cao, "Coil temperature rise and workpiece forming efficiency of electromagnetic forming based on half-wave current method," *IEEE Access*, vol. 8, pp. 9371–9379, 2020, doi: 10.1109/ACCESS.2020.2965254.
[18] L. Qiu, Y. Li, Y. Yu, Y. Xiao, P. Su, Q. Xiong, J. Jiang, and L. Li, "Numerical and experimental investigation in electromagnetic tube expansion with axial compression," *Int. J. Adv. Manuf. Technol.*, vol. 104, nos. 5–8, pp. 3045–3051, Aug. 2019.
[19] Z. L. Li, W. J. Qiao, and X. X. Tao, "Current interaction," (in Chinese), *J. Hubei Univ. Technol.*, vol. 15, no. 2, pp. 68–70, 2000.
[20] M. V. Lankin, O. I. Lozin, and M. Y. Lankina, "Magnetization dynamic characteristics models for hydraulic drives of proportional electromagnets," *Procedia Eng.*, vol. 206, pp. 443–448, Jan. 2017.
[21] C. Shao, "Parametric simulation and analysis of the suction characteristics of proportional electromagnets," (in Chinese), M.S. thesis, School Machinery Automat., Wuhan Univ. Sci. Technol., Wuhan, China, 2015.
[22] L. Li, "Study on directional solidification texture and phase change texture of pure iron," (in Chinese), M.S. thesis, Adv. Mater. Res. Center, Xiangtan Univ., Xiangtan, China, 2006.
[23] W. Han, L. Xiong, and Z. Yu, "Braking pressure control in electro-hydraulic brake system based on pressure estimation with nonlinearities and uncertainties," *Mech. Syst. Signal Process.*, vol. 131, pp. 703–727, Sep. 2019.
[24] F. P. E. Ngak, G. E. Ntamack, and L. Azrar, "Dynamic and static behaviors of multilayered angle-ply magnetoelectroelastic laminates with viscoelastic interfaces," *Composite Struct.*, vol. 189, pp. 667–687, Apr. 2018.
[25] D. Tlalolini, M. Ritou, C. Rabréau, S. Le Loch, and B. Furet, "Modeling and characterization of an electromagnetic system for the estimation of frequency response function of spindle," *Mech. Syst. Signal Process.*, vol. 104, pp. 294–304, May 2018.
[26] L. Gao, C. Wu, D. Zhang, X. Fu, and B. Li, "Research on a high-accuracy and high-pressure pneumatic servo valve with aerostatic bearing for precision control systems," *Precis. Eng.*, vol. 60, pp. 355–367, Nov. 2019.
[27] H.-W. Li, S.-L. Yan, M. Zhan, and X. Zhang, "Eddy current induced dynamic deformation behaviors of aluminum alloy during EMF: Modeling and quantitative characterization," *J. Mater. Process. Technol.*, vol. 263, pp. 423–439, Jan. 2019.
[28] L. Qiu, Y. Li, Y. Yu, A. Abu-Siada, Q. Xiong, X. Li, L. Li, P. Su, and Q. Cao, "Electromagnetic force distribution and deformation homogeneity of electromagnetic tube expansion with a new concave coil structure," *IEEE Access*, vol. 7, pp. 117107–117114, 2019, doi: 10.1109/ACCESS.2019.2923264.
[29] Y. Lu, Z. Zuo, C. Zhao, F. Zhang, and M. Du, "Study on dynamic characteristics and control algorithm design for fuel metering valve of high-pressure pump," *IFAC-PapersOnLine*, vol. 51, no. 31, pp. 930–935, 2018.
[30] P. Naseradinmousavi, "Nonlinear modeling, dynamic analysis and optimal design and operation of electromechanical valve systems," Ph.D. dissertation, Dept. Mech. Eng., Villanova Univ., Villanova, PA, USA, 2012.
[31] S. Zhang, T. Minav, M. Pietola, H. Kauranne, and J. Kajaste, "The effects of control methods on energy efficiency and position tracking of an electro-hydraulic excavator equipped with zonal hydraulics," *Autom. Construct.*, vol. 100, pp. 129–144, Apr. 2019.
[32] W. Duan, Z. Yan, W. Luo, P. Zhang, Z. Gui, Z. Wang, and Y. Wang, "Experimental study of thrusts of a cylindrical linear synchronous motor with an HTS coil magnet as the excitation system," *Phys. C, Supercond. Appl.*, vol. 508, pp. 1–5, Jan. 2015.

FANGWEI XIE was born in Anhui, China, in 1983. He received the B.S. and Ph.D. degrees in mechanical engineering from the China University of Mining and Technology, in 2006 and 2010, respectively.

From 2011 to 2014, he was a Lecturer with Jiangsu University, China, where he was also an Associate Professor, from 2014 to 2019. Since 2019, he has been a Professor with the China University of Mining and Technology. He is the author of more than 80 articles, and more than 40 inventions. His research interests include fluid power transmission and control, compound transmission and its energy saving technology, and vehicle suspension system design and control and its applications.

Dr. Xie is a member of American Society of Mechanical Engineer, evaluation expert of National Natural Science Foundation, and he is a reviewer of many journals. He received the 2019 Emerald Highly Commended Award and the science and technology progress awards many times.

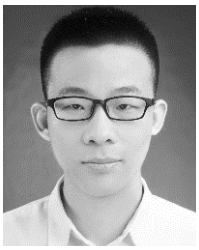

RUI ZHOU was born in Jiangsu, China, in 1994. He is currently pursuing the M.S. degree in mechanical engineering at Jiangsu University, Zhenjiang, China. His main research interest includes continuous damping control shock absorber.

DENGSHUAI WANG was born in Jiangsu, China, in 1993. He received the M.S. degree in mechanical engineering from Jiangsu University, Zhenjiang, China, in 2019. His main research interest includes output characteristics of proportional valve with adjustable damping shock absorber.

JUN KE was born in Jiangsu, China, in 1993. He is currently pursuing the M.S. degree in mechanical engineering at Jiangsu University, Zhenjiang, China. His main research interest includes mechanical design and cooling systems of high-power charging pile.

XINJIAN GUO was born in Shandong, China, in 1993. He received the M.S. degree in mechanical engineering from Jiangsu University, Zhenjiang, China, in 2019. His main research interests include fluid power and wet clutch transmission mechanism.

VAN XO NGUYEN was born in Thai Binh, Vietnam, in 1980. He received the Ph.D. degree in mechanical engineering from the China University of Mining and Technology, in 2013.

From 2004 to 2019, he was a Lecturer with the Hanoi University of Mining and Geology, Vietnam, where he has been the Head of the Department of Machine and Industrial Equipment, Faculty of Electro-Mechanics, since 2016. He is the author of more than 30 articles, scientific research topics and books. His research interests include fluid power transmission and control, and mechanical vibration and its application.

Dr. Nguyen received the certificate of merit from the Minister of Education and Training of Vietnam, in 2019.